Desalination and Water Treatment
www.deswater.com
doi: 10.5004/dwt.2021.27270

226 (2021) 197–207
June

Sorption behavior of perfluorooctane sulfonate on hydrous ferric oxide from aqueous solution

Ji Zang[a,†], TianTian Wu[a,†], Jun Yang[a], Zhengxin Xie[a,b], Shisuo Fan[a,b], Jun Tang[a,b,*]

[a]*School of Resource and Environment, Anhui Agricultural University, Hefei 230036, China, Tel./Fax: +86551 65786790; emails: 18895688872@163.com (J. Zang), wu18365280208@163.com (T.T. Wu), anhuinongye@163.com (J. Yang), xiezx@ahau.edu.cn (Z.X. Xie), fanshisuo@ahau.edu.cn (S.S. Fan)*
[b]*Hefei Scientific Observing and Experimental Station of Agro-Environment, Ministry of Agriculture, China, Tel./Fax: +86551 65786790; email: tj2192@ahau.edu.cn*

Received 1 December 2020; Accepted 26 March 2021

ABSTRACT

Perfluorooctane sulfonate (PFOS) has increasingly attracted global concern in recent years because of its ubiquitous distribution and strong bioaccumulation. Hydrous ferric oxide (HFO) is an important compound in soil and sediment with reactive surfaces and its effect on the sorption behavior of PFOS in the environment was unclear. In this study, HFO was prepared and was characterized by surface area and porosity analysis, X-ray photoelectron spectroscopy, Fourier transform infrared spectroscopy. Then, the influence of pH, cations, and anions on the adsorption of PFOS on HFO was investigated. The results have shown that PFOS adsorption was highly pH-dependent. When the pH exceeded 8.74, the removal rate of PFOS decreased significantly. A high concentration of cation and anions had a strong inhibitory effect on PFOS adsorption by hydrous ferric oxide. The sorption process of PFOS on HFO followed pseudo-second-order kinetics, and the Temkin model well described the sorption equilibrium experiments. The intraparticle diffusion model suggests that two steps control the adsorption process and that the intraparticle diffusion model largely dominated the adsorption process. The maximum adsorption capacity of PFOS on HFO could reach 157.9736 mg g^{-1}. The mechanisms of PFOS sorption onto HFO included electrostatic interactions, surface complexation and hydrogen bonding. Therefore, PFOS can be effectively adsorbed onto HFO in water, and the transfer behavior of PFOS would be affected by HFO in water with solution condition variation.

Keywords: Hydrous ferric oxides; Perfluorooctane sulfonate; Adsorption; Models; Mechanisms

1. Introduction

Perfluoroalkyl substances (PFASs) are anionic surfactants with a stable carbon–fluorine (C–F) bond, and the stable carbon–fluorine bonds result in their persistence in the environment [1]. Perfluorooctane sulfonate (PFOS), one of the most common PFAS, together with its salts, have been listed under the Stockholm Convention as persistent organic pollutants; this restricted its global use and production [2–4]. PFOS, which is derived from the large production of PFOS-related compounds, has increasingly attracted global concern in recent years because of its ubiquitous distribution, persistence, strong bioaccumulation, and potential toxicity [5,6], PFOS and related substances are still used and manufactured in China because of the lack of cost-effective alternative technologies [7]. Direct emissions from PFOS-containing products have released 450–2,700 tons of PFOS into the aquatic environment [8]. Because of the hydrophobic and hydrophilic functionalities of PFASs, they are expected to behave differently from traditional

* Corresponding author.

† These authors contributed equally to this work.

non-ionizable organic pollutants [9,10]. Adsorption by soil or sediment determines the fate and behavior of PFASs in the environment [11–13], and the organic carbon content and pH are important factors for adsorption [14,15].

Hydrous ferric oxide (HFO) is an important compound substance in natural waste with reactive surfaces [16,17], further influencing the sorption behavior of pollutants in water. Due to its strong adsorption capacity to phosphate [17], arsenic [18,19], heavy metals [20], and antibiotics [21], HFO plays a key role in the transfer behavior of contaminants in water [22,23]. However, very limited information has been available on the adsorption of PFOS onto mineral surfaces [24], especially for the adsorption mechanism. Thus, more research insight into the process of HFO adsorption of PFOS is still needed in order to better understand the potential effect of HFO on PFOS mobility in aquatic environments.

The purpose of this study is to evaluate the adsorption behavior and mechanisms of PFOS onto HFO in an aqueous solution. The physical and chemical properties of HFO samples were characterized by Fourier transform infrared (FTIR) spectroscopy, X-ray photoelectron spectroscopy (XPS). The behavior of PFOS onto HFO adsorption was investigated systematically through batch adsorption experiment isotherms, and the adsorption kinetics, isotherms, and thermodynamics were explored.

2. Materials and methods

2.1. Chemicals

Methanol (HPLC grade) and acetonitrile (HPLC grade) were obtained from Tedia (Fairfield, OH, USA). PFOS with the purity of 98% was obtained from ANPEL Laboratory Technologies Inc., (Shanghai, China). PFOS solutions with different concentrations were prepared using ultrapure Milli-Q water to simulate contaminated water. Ferric chloride hexahydrate ($FeCl_3{\cdot}6H_2O$) and $MgCl_2{\cdot}6H_2O$ were bought from Sinopharm Chemical Reagent Co., Ltd., (China). All other chemicals used (including NaOH, HCl, NaCl, NaF, $NaNO_3$, and $CaCl_2{\cdot}2H_2O$) were of reagent grade and were purchased from Xilong Scientific Co., Ltd., (Guangzhou, China). Water was prepared using the Milli-Q Plus ultrapure water system (Billerica, MA, USA).

2.2. Preparation of HFO

HFO was synthesized following a procedure similar to that described by Zhang et al. [25]. The synthesis of HFO was as follows: $FeCl_3{\cdot}6H_2O$ (0.8 mol L^{-1}) was dissolved in deionized water under vigorous magnetic stirring, and then NaOH solution was slowly added into the $FeCl_3{\cdot}6H_2O$ solution, with the solution pH value maintain at 7.0 ± 0.5. After addition, the formed suspension was continuously stirred for 1 h and aged at room temperature for 24 h. The precipitated HFO particles were collected by centrifugation and then were washed several times with ultra-pure Milli-Q (MQ) water to remove residual ions. Finally, the HFO was freeze-dried in a freeze-dryer, ground in an agate mortar, and then passed through a 200-mesh sieve. The screened HFO was collected and stored in a brown glass bottle. The basic properties of the resultant sorbent are available in Table 1.

Table 1
Adsorption kinetics parameters of PFOS onto HFO

Pseudo-first-order		Pseudo-second-order	
q_e (mg g^{-1})	19.39	q_e (mg g^{-1})	19.94
k_1 (min^{-1})	0.1161	k_2 (g (mg min)$^{-1}$)	0.01107
R^2	0.6213	R^2	0.9540
Two-compartment equation		Intraparticle diffusion model	
q_e (mg g^{-1})	19.70	k_{i1} (mg g^{-1} $min^{0.5}$)	0.5445
F_{fast}	0.6447	k_{i2} (mg g^{-1} $min^{0.5}$)	0.0584
F_{slow}	0.3553	C_{i1} (mg g^{-1})	14.05
k_{fast} (min^{-1})	15.00	C_{i2} (mg g^{-1})	18.62
k_{slow} (min^{-1})	0.02860	R_{i1}^2	0.9718
R^2	0.9447	R_{i2}^2	0.5115

2.3. Experimental set-up

Stock standard solutions of 1,000 mg L^{-1} PFOS in methanol were prepared and stored in polypropylene (PP) tubes in the refrigerator at 4°C In the adsorbent dosage experiment, 80 mL of PFOS solution with a concentration of 5 mg L^{-1} was added to a 100 mL PP centrifuge tube. The pH value was adjusted to 5.5 with hydrochloric acid and sodium hydroxide, and then 0.05, 0.1, 0.2, 0.3, and 0.5 g L^{-1} of HFO were added to the centrifuge tubes. Each centrifuge tube was placed on a constant-temperature oscillator. The temperature was controlled at 25°C, and the frequency of the oscillator was set at 150 rpm. Samples were periodically withdrawn to determine the residual concentration of PFOS in the solution. The amounts of PFOS adsorbed at specific durations were determined using Eq. (1).

$$\text{Adsorption capacity: } q_e = \left(C_e - C_t\right) \times \frac{V}{m} \tag{1}$$

where q_e is the adsorption amount at equilibrium time (mg g^{-1}), V is the volume of solution (L), and m is the mass of adsorbent (g).

To study the effect of contact time on PFOS removal by HFO, the interval times for sample collection were set as 10, 20, 30, 40, 60, 90, 120, 180, 240, 300, 480, and 720 min. The concentration of PFOS in the filtrate was determined, and the removal rate of the sample was calculated. Other conditions were the same as the adsorption experiment. Finally, the adsorption kinetics of PFOS on the HFO samples were fitted by the following models: pseudo-first-order, pseudo-second-order, two-compartment first-order, and intraparticle diffusion models. The adsorption kinetic equations are listed in supporting information.

To measure the adsorption isotherm, the equilibrium data obtained for initial PFOS concentration variation from 1 to 20 mg L^{-1} on PFOS adsorption capacity were studied by widely applied Langmuir and Freundlich adsorption isotherm models at 25°C, 35°C, and 45°C. Other conditions were the same as those for the adsorption experiment. The adsorption isotherm equations are listed in supporting information.

To study the effect of initial pH and cation on PFOS adsorption, absorbents were buffered in PFOS solution

at different pH values (from 3.0 to 11.0) by adjusting with 0.1 mol L^{-1} HCl or NaOH solution. Cation strength ranging from 0 to 1.5 mol L^{-1} were prepared with Na^+ or Mg^{2+}. Other conditions was the same as those for the adsorption experiment.

The effect of competing anions on PFOS adsorption was obtained by competing-anion experiments with individual anions (Cl^-, SO_4^{2-}, F^-, and NO_3^-) present in the Na^+ ion solution, varied in the range of 0 to 10 mmol L^{-1}.

Each group of the above experiments was set with three parallels and averaged.

2.4. Characterization methods

The functional groups of HFO before and after adsorption were measured by FTIR spectroscopy (Thermo Fisher Scientific Co., Waltham, MA, USA). Binding energies were determined by XPS (Thermo Fisher Scientific ESCALAB 250Xi, USA). The specific surface area, pore-volume, and pore size of the HFO were determined using a surface area and porosity analyzer (Micromeritics TriStar II 3020; Atlanta, GA, USA) at 77 K under a N_2 atmosphere. The pH of zero point charges (pH_{PZC}) of the HFO was measured based on the previous study [26].

2.5. Measurement of PFOS

After the adsorption experiments, the supernatants were collected after centrifugation at 10,000 rpm for 5 min, and 0.1 mL of sample solution was diluted with 0.9 mL of water containing 50% methanol (v/v = 1/9). The concentrations of PFOS were determined using a Waters ACQUITY UltraPerformance LC System (UPLC/MS) equipped with a 100 × 2.1 mm ACQUITY UPLC BEH C18 column (1.7 μm particle size) and tandem quadrupole mass spectrometers (Xevo Waters, Milford, MA). The mobile phase was composed of 5 mM ammonium acetate in water (A) and 0.1% (v/v) formic acid in methanol (B), and a gradient program of 60% A in 0–2 min, 10% A in 2–3 min, and 60% A in 3–5 min was used. The flow rate was maintained at 0.3 mL min^{-1}, and the column temperature was held at 40°C. The injection volume was 5 μL, and the cone voltage and collision energy were 60 and 39 V, respectively.

2.6. Quality assurance/quality control

Solvent blanks consisting of methanol and 5 mM ammonium acetate (1:1, v/v) were injected every 10 samples, and no interference was observed. Field blanks were prepared to check possible laboratory contamination. Procedural blank samples prepared with the experiment process were also run after every 10 samples to ensure that sample processing materials and procedures were free of contamination.

3. Results and discussion

3.1. Characterization of HFO

The specific surface area, pore-volume, and pore size of the HFO were 226.796 m^2 g^{-1}, 0.167 cm^3 g^{-1}, and 3.495 nm, respectively. Thus, the developed pore structure and large specific surface area of HFO were beneficial for PFOS adsorption.

The XPS spectra of HFO are displayed in Fig. 1. XPS can be applied to analyze the functional groups on adsorbent [27–29]. Functional groups of different elements can be obtained by peak-splitting fitting. The fitted O 1s XPS spectrum presented three peaks at 529.75, 531.29, and 532.88 eV attributed to Fe–O, Fe–OH, and –OH, respectively. After PFOS adsorption, the area ratio for the peak at 531.29 eV related to Fe–OH increased from 31.9% to 53.9%, and the peak at 532.88 eV related to OH decreased

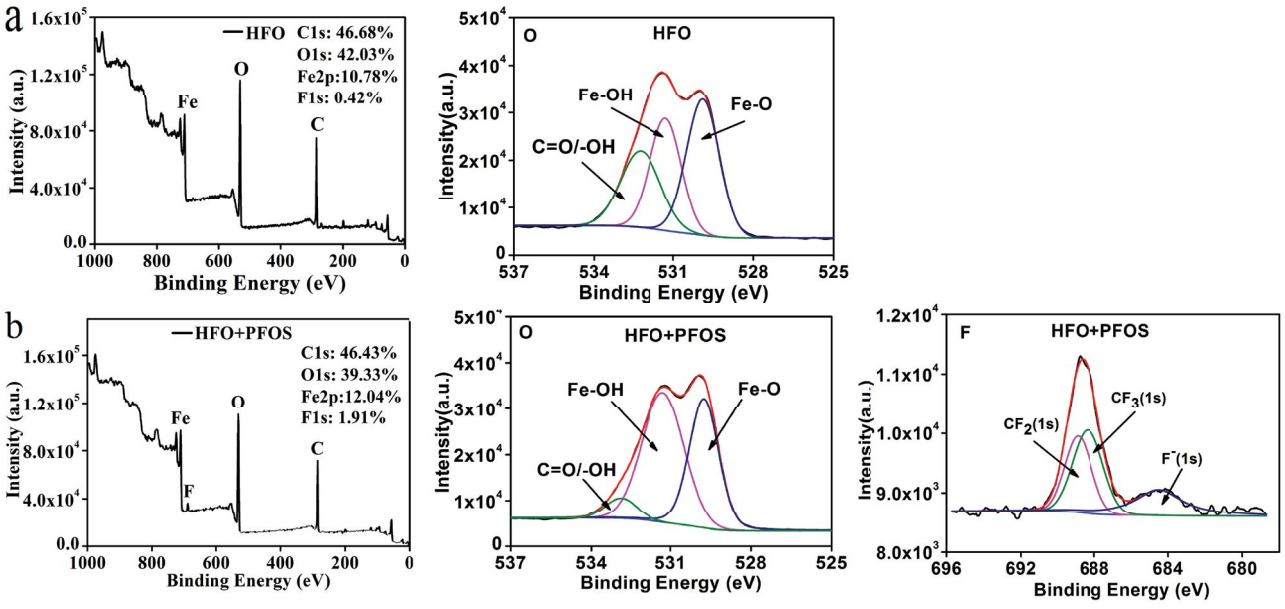

Fig. 1. XPS of HFO before (a) and after (b) PFOS removal.

from 27.7% to 6.2%. Surface hydroxyl groups on the HFO participated in the adsorption of PFOS and possibly hydrogen bonds at its surface, as confirmed by the results of XPS analysis. According to the XPS analysis before and after action, the position and area of peaks of O–, F–, and Fe–containing groups changed. Therefore, the XPS analysis revealed that PFOS had been successfully adsorbed to HFO and that Fe– and O– containing groups may be involved in the removal of PFOS.

The FTIR spectra are displayed in Fig. 2. The marked differences for the HFO peak at 3,398 cm^{-1} and the HFO + PFOS peak at 3,406 cm^{-1} were attributed to the stretching vibration of the –OH group, which indicated significant hydrogen-bonding interactions [30,31]. The peaks of aromatic CO– (1,249 cm^{-1}) became more intense, indicating that the concentration of oxygen bonded to C on the HFO surfaces increased and that PFOS thus adsorbed on the HFO surface. The bands at 474 and 1,625 cm^{-1} were respectively assigned to the stretching vibration of Fe–O groups and –COOH stretching vibrations of amides [32]. The FTIR spectra of HFO before and after the reaction are presented in Fig. 2. The peaks shifted from 3,398; 1,625; 1,252–3,406; 1,626, and 1,249 cm^{-1} after PFOS adsorption on HFO. This indicates that –OH, –COOH, and –COH functional groups may participate in the interaction between PFOS and HFO. The main mechanisms may involve surface complexation, including hydrogen bonding and electronic interactions.

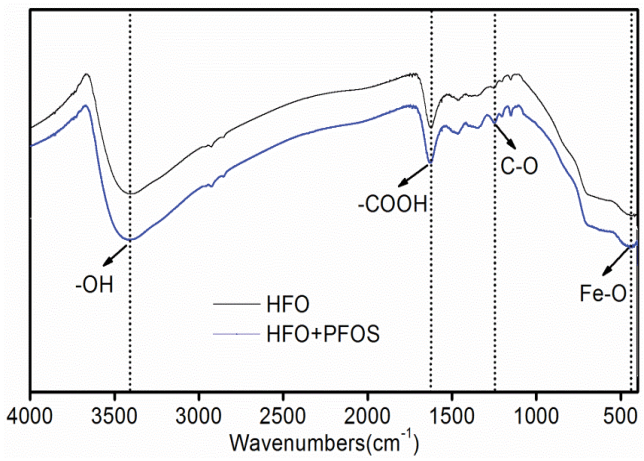

Fig. 2. FTIR spectra of HFO before and after PFOS removal.

3.2. Adsorption behavior

The effect of HFO dosage on the removal rate of PFOS is shown in Fig. 3a. The HFO dosage increase from 0.05 to 0.2 g L^{-1} resulted in an increase in the removal percentage of PFOS from 32.6% to 88.0%. With the increase in the amount of adsorbent, the surface area and exchange sites increase, leading to an increase in the removal percentage of PFOS [33]. According to these results, the rapid increase in PFOS removal by HFO occurred in the range of 0.05 to 0.2 g L^{-1}, but it leveled off and attained equilibrium as we further increased the HFO loading (ranging from 0.2 to 0.5 g L^{-1}). Increasing the adsorbent dosage above 0.2 g L^{-1} had a trivial effect on the increase in removal percentage of PFOS. This may be attributed to the interaction of particles at higher solid/liquid ratios or to the aggregation of particles. When the HFO dosage was 0.2 g L^{-1}, the inflection point appears, and the removal rate reaches 90%; after this further increase in the adsorbent, the mass did not affect the removal rate. On the basis of the removal effect and economy, the optimum absorbent dosage was 0.2 g L^{-1}.

The influence of initial pH on PFOS removal is shown in Fig. 3b. As seen in Fig. 3b, HFO uptake retained a higher level in a wide pH range, from 3.15 to 8.74. At higher pH levels (from 8.74 to 10.98), the removal rates of PFOS by HFO decreased. This may be caused by the decrease in surface charge of HFO due to the neutralization of positive charge with OH^- as long as electrostatic interactions. However, with the increase in pH value from 6.57 to 8.74, the removal rate of PFOS increased slightly. The point of zero charge of HFO was around 7.8 (as shown in Fig. S1). The pKa of PFOS is -3.72 [34], indicating that PFOS is negatively charged. When the pH value exceeded 8.74, the removal rate of PFOS decreased significantly (from 88% to 14%). This may be because the surface charge of HFO was surrounded by negative charge, and PFOS was electrostatically repelled.

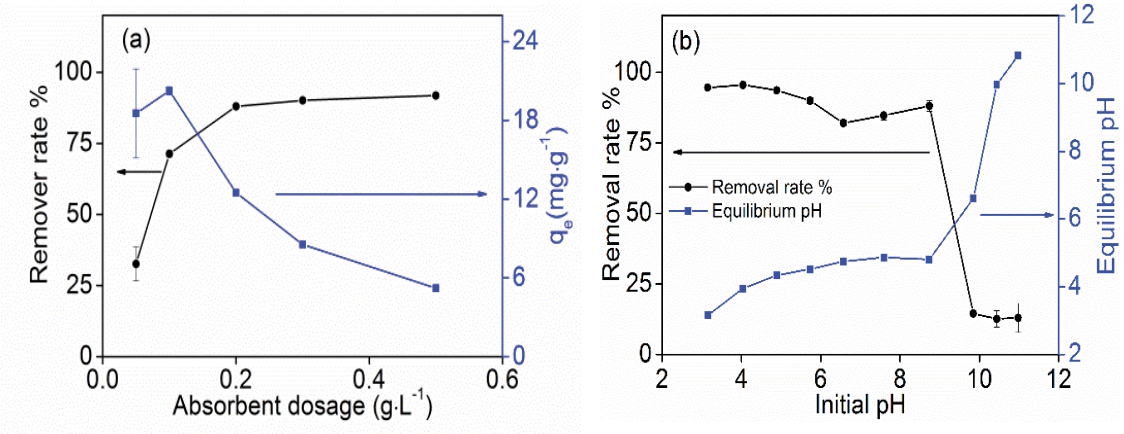

Fig. 3. Effect of absorbent dosage (a) and pH (b) on the absorption of PFOS onto HFO.

The relationship between the initial pH and equilibrium pH of the PFOS adsorption process is displayed in Fig. 3b. When the initial pH was 3.15–8.74, a slight change occurred at equilibrium pH, which can be explained by the buffering capacity of the HFO system. With further increase of the initial solution pH values to strong-alkali conditions (pH = 9.85–10.98), the HFO showed limited buffer capacity, and it lost the buffering completely at pH_I = 10.98. A similar phenomenon was also observed by Hu et al. [35].

This comparison indicates that the adsorption behavior of PFOS onto HFO may be principally due to the electrostatic interaction. It has been previously reported the surface charge of nano-sized alumina has significant effects on its removal by PFOS [36]. As mentioned above, pH was an important effect factor in the removal of PFOS by HFO.

In addition to pH, the effects of cation type and ionic strength in the solution are also important in the adsorption of PFOS on HFO. Figs. 4a and b show the effect of different concentrations of cations (Na^+ and Mg^{2+}) in the adsorption of PFOS on HFO. It indicates a decreasing and then increasing trend of PFOS adsorption with the increase in Na^+ and Mg^{2+} concentrations. A possible explanation of this result is that lower ionic strength causes the potential hindering effect due to the competitive adsorption of chloride ions on the active adsorption sites, which may also decrease PFOS adsorption on the HFO [37], as well as the sorption capacities of PFOS on the adsorbents, such as boehmite [38], chitosan [39], and resins [40]. With the increase in ion concentration, the influence of competitive adsorption gradually decreases, and the increase in cation concentration reduces the electrostatic repulsion between PFOS and increases the adsorption of PFOS [24,41,42]. The effect of magnesium chloride on PFOS adsorption was less than that of sodium chloride. These phenomena could be explained by the salting-out effect and the effect of bridges that Mg^{2+} formed between carboxyl groups [43,44]. These observations indicated that the predominant mechanism for PFOS adsorption on the HFO included electrostatic interaction.

Considering that PFOS is mostly negatively charged in wastewater, it is important to investigate the possible competitive effects of competing anions on the adsorption of PFOS. The effects of four common anions, Cl^-, SO_4^{2-}, F^-, and NO_3^- (up to 10 mmol L^{-1}), were studied for HFO. On goethite, SO_4^{2-} predominantly forms monodentate inner-sphere surface complexes at pH < 6 [45]; F^-, Cl^-, and NO_3^- can only form outer-sphere complexes with ferric oxides [46], whereas the PFOS sulfonate group forms outer-sphere complexes and possibly hydrogen bonds at the mineral surface [47]. Fig. 4c shows an obvious decline in the PFOS adsorption capacity for all HFO with the increase of ions concentration ranged from 0 to 10 mmol L^{-1}. As can be seen from the figure, a low concentration of fluorine ion has a strong inhibitory effect on PFOS adsorption by iron hydrate oxide, with a removal rate of only about 40%. It may be that fluorine ion has strong electronegativity and that Fe has a strong and specific affinity to fluoride [48]. Adsorption competition with PFOS is strong, and so fluorine ion at low concentration has a strong inhibitory effect. Meanwhile, SO_4^{2-} exerts the strongest competition effect because the ionic strength of the divalent ion is much larger than that of monovalent Cl^-, F^-, or NO_3^-, at the same concentration (except 0.5 mmol L^{-1}). The degree of anion interaction increased with an increase in their concentrations within 0.5–10 mmol L^{-1} in the solution. The inhibition of PFOS adsorption follows the following order: $SO_4^{2-} > F^- > Cl^- > NO_3^-$.

The adsorption kinetics of PFOS on HFO is shown in Fig. 5, which manifests that adsorption activity proceeded quickly in the first 3 h, probably because of the availability of abundant active sites on the HFO surface. The amount of adsorbed PFOS increased slowly in the final stage of the PFOS adsorption reaction, resulting in a decrease in active sites, similar to the finding reported by Tang et al. [24] and Wang et al. [43]. In order to investigate the rate or mechanism of PFOS adsorption onto HFO, the experimental kinetic data were fitted to kinetic models (e.g., pseudo-first-order, pseudo-second-order, intraparticle diffusion, and two-compartment first-order models). The resulting curves and kinetic parameters are shown in Fig. 5 and are given in Table 1. The correlation coefficient (R^2) suggests that the pseudo-second-order model (R^2 = 0.954) and two-compartment first-order model (R^2 = 0.945) better fitted the experimental data as compared with the Elovich model (R^2 = 0.87) and the pseudo-first-order model (R^2 = 0.621). The pseudo-second-order equation and the two-compartment first-order model suggest that chemisorption occurred between PFOS and HFO, involving the exchange of electrons or valency forces through sharing between sorbent and sorbate [47,49,50].

The two-compartment first-order model also offered a good fit of the data, although it was inferior to the pseudo-second-order rate model. It is observed that the two-compartment first-order model described the adsorption

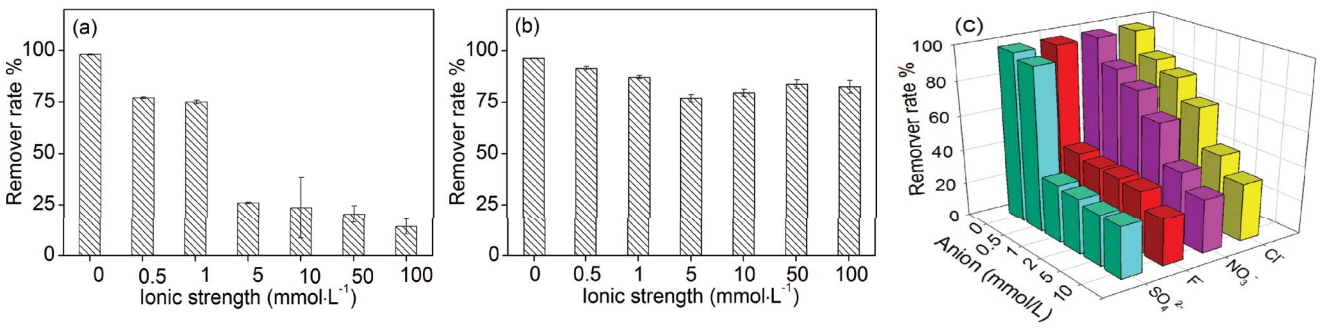

Fig. 4. Effect of Na^+ ionic strength (a), Mg^{2+} ionic strength (b), anions types and strength (c) on adsorption of PFOS.

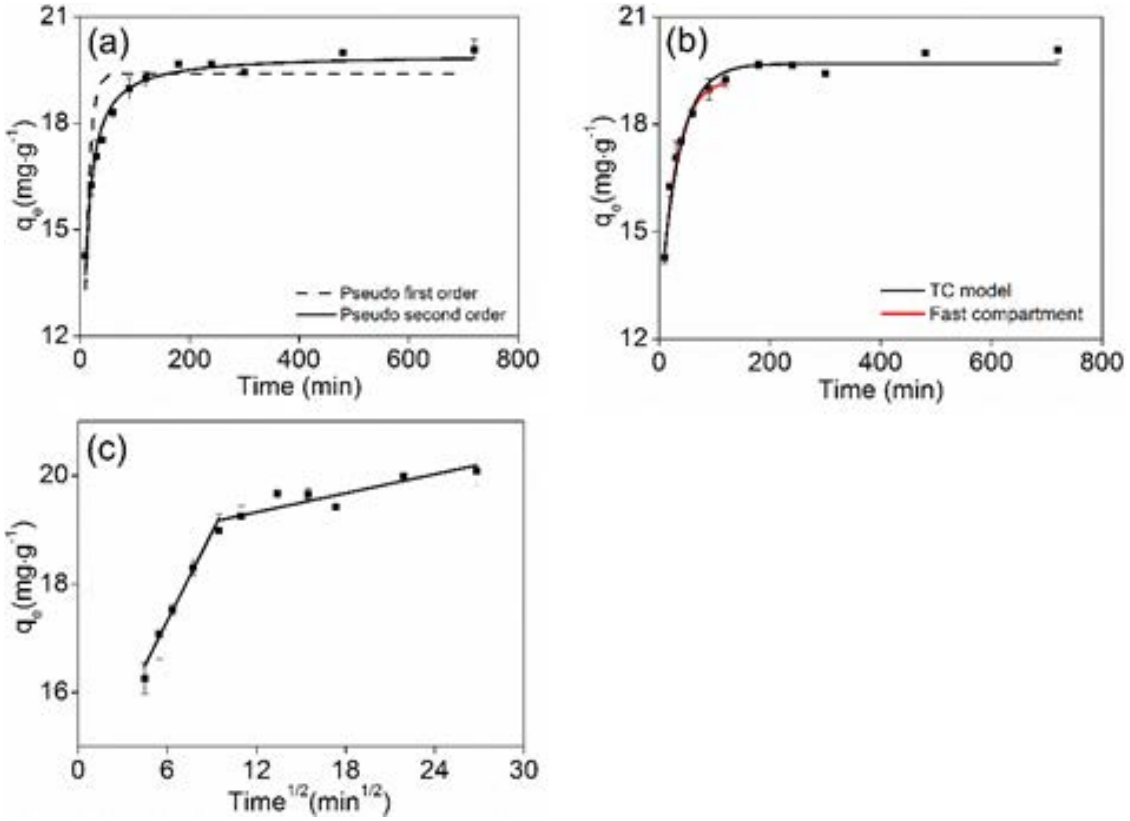

Fig. 5. Kinetics of PFOS sorption onto HFO by fitting the pseudo-first-order and pseudo-second-order model (a), two-compartment first-order equations model (b), intraparticle diffusion model (c).

of PFOS by HFO as a two-domain process. As illustrated in Fig. 5b, the fast compartment made a predominant contribution to the total sorption amount in the whole process, with a relatively short time of about 120 min. The fast compartment reached around 95.8% of the equilibrium adsorption capacity by HFO. It is commonly recognized that the hydrogen bond between the hydroxyl groups in PFOS molecules and iron–oxygen groups on the HFO surface causes the fast sorption of PFOS [10,51].

The intraparticle diffusion models explicitly show double adsorption stages. This suggests that two steps control the adsorption process and that intraparticle diffusion did not solely dominate adsorption, but rather largely dominated the adsorption of HFO onto PFOS ($k_{i1} > k_{i2}$) [52,53].

The sorption isotherms of PFOS on HFO is displayed in Fig. 6. The R^2 value suggests that the Temkin model (R^2 = 0.91–0.97) better fitted the experimental data as compared with the Freundlich (R^2 = 0.80–0.90), Langmuir (R^2 = 0.85–0.97), and Dubinin–Radushkevitch isotherm (R^2 = 0.86–0.97) models, as seen in the R^2 values in Table 1. The Temkin isotherm model mainly describes the chemical adsorption process as electrostatic interaction [54]. In the present study, therefore, electrostatic interaction is a mechanism affecting the interaction between PFOS and HFO [55]. This result supports the obtained result from adsorption kinetics.

Table 2 results show that the values for the bonding energy (E_a) derived from the Dubinin–Radushkevitch isotherm model equation at the three temperatures were lower than 8 kJ mol^{-1}. This indicates that the adsorption of PFOS onto HFO is a physical adsorption process [56]. The n values derived from the Freundlich equation at the three temperatures were greater than unity, indicating the favorable PFOS adsorption onto HFO and the physical adsorption of PFOS by HFO [57]. Langmuir's model also offered a good fit of the data (R^2 = 0.85–0.97), although inferior to that of the Temkin model. This implies that the adsorption of PFOS on HFO main involves a monolayer. As shown in Fig. S2, $R_L = 1/(1 + C_e b)$ in the present study was larger than 0 and smaller than 1, indicating that the adsorption of PFOS on HFO was favorable [30]. This result supports the obtained result from the Freundlich model. The R^2 values of all sorption isotherms were relatively small for PFOS sorption on HFO, suggesting that other interaction mechanisms (such as hydrophobic interaction [24,58]) may also be present in the sorption processes. Therefore, this adsorption phenomenon was considered as physisorption with heterogeneous adsorption [59].

Compared with other previous adsorbents in Table 3, the maximum adsorption capacity of PFOS on HFO was considerable. The adsorbent used in this research showed environment friendly, higher adsorption capacity and cost-effectiveness compared with other adsorbents. Thus, the adoption of HFO for the preparation of adsorbent for PFOS removal from aqueous solutions shows promising future.

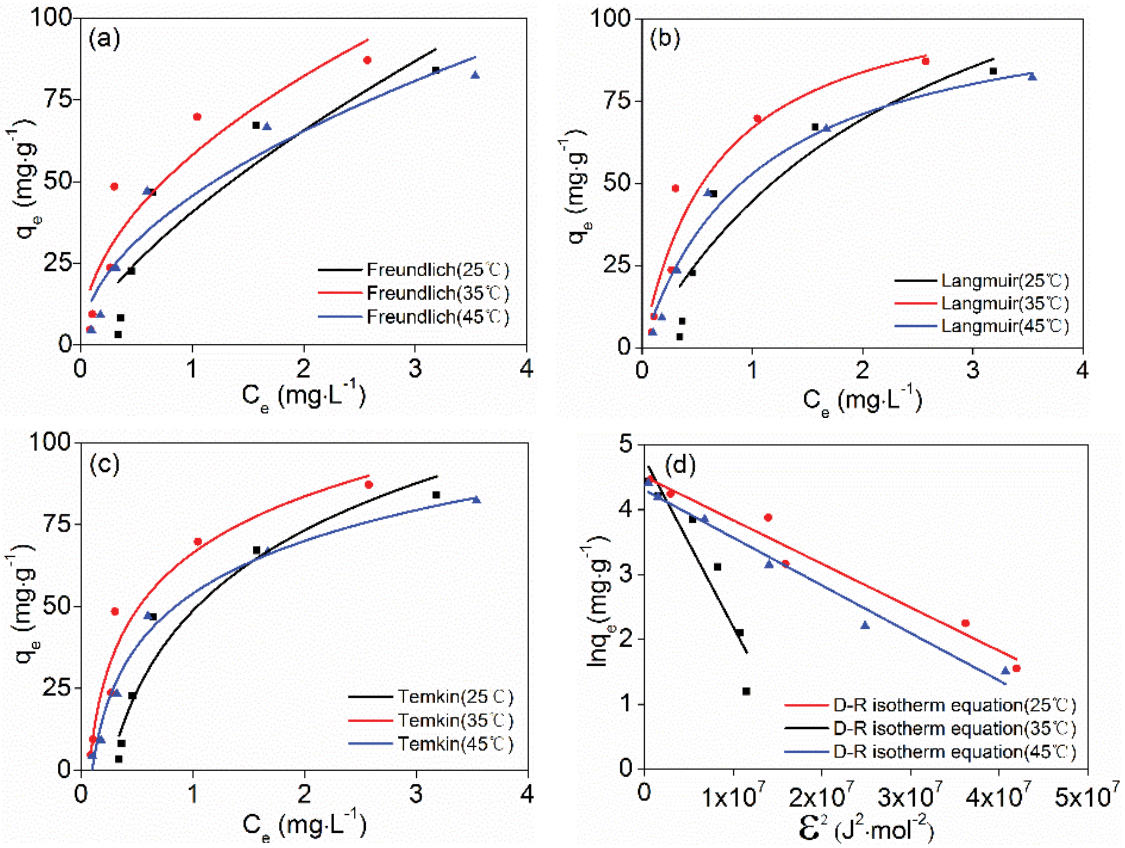

Fig. 6. Freundlich isotherm model (a), Langmuir isotherm model (b), Temkin isotherm model (c) and Dubinin–Radushkevitch model (d) for PFOS adsorption on HFO.

Table 2
Parameters corresponding to adsorption isotherm models

Models	298 (K)	308 (K)	318 (K)
Langmuir model			
K_L (L mg^{-1})	0.3939	1.4709	0.9576
q_m (mg g^{-1})	158.0	112.4	108.2
R^2	0.8486	0.9207	0.9672
Freundlich model			
K_F ((mg g^{-1})(L mg^{-1})$^{1/n}$)	40.63	58.06	45.57
n	1.446	1.992	1.918
R^2	0.8007	0.8448	0.8988
Temkin model			
A_T	3.964	14.38	10.28
R	8.314	8.314	8.314
B_T	70.00	102.9	114.1
R^2	0.9304	0.9443	0.9784
Dubinin–Radushkevitch isotherm model			
q_m (mg g^{-1})	119.1	90.92	73.70
β_{DR} (mol^2 J^{-2})	25.83 × 10^{-8}	6.716 × 10^{-8}	7.347 × 10^{-8}
R^2	0.8638	0.9584	0.9733
E_a (kJ mol^{-1})	1.391	2.729	2.609

Table 3
Comparison of the adsorption capacity of different adsorbent with HFO

Adsorbent	Adsorption capacity (mg g^{-1})	Reference
Alumina	0.022	[44]
Boehmite	0.263	[38]
AC-H_3PO_4	75.13	[60]
AC	138	[27]
Corn straw-derived biochar	169.3	[61]
HFO	157	Present study

3.3. Adsorption mechanisms

According to the results of pH (Fig. 3b), ionic strength (Fig. 4), and sorption isotherms (Fig. 6), electrostatic interaction is a present mechanism affecting the interaction between PFOS and HFO.

Based on the results of adsorption kinetics, the adsorption process involved physical processes and chemical bonding. The adsorption process included external liquid film diffusion and intraparticle diffusion processes, but intraparticle diffusion largely dominated the adsorption of HFO onto PFOS ($k_{i1} > k_{i2}$).

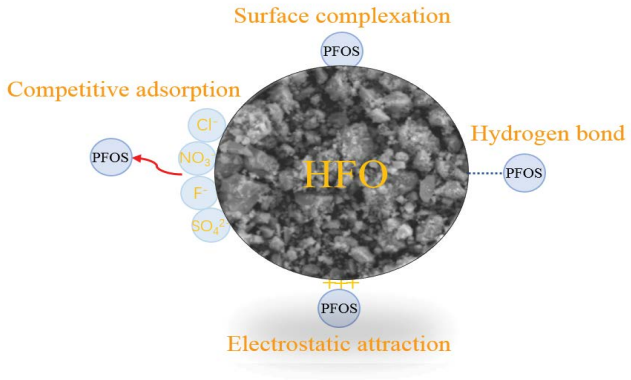

Fig. 7. Schematic diagram of mechanisms for PFOS adsorption on HFO.

According to XPS and FTIR analysis (Figs. 1 and 2), the mechanisms of adsorption PFOS onto HFO refer to electrostatic interaction, surface complexation, and hydrogen bonding. –OH, –COOH, C–O, and Fe–O functional groups are likely to participate in PFOS binding.

From the above analysis, the adsorption mechanism of PFOS onto biochar involves electrostatic interaction, intraparticle diffusion, surface complexation, and hydrogen bonding.

A schematic diagram of mechanisms for PFOS adsorption on HFO is shown in Fig. 7.

4. Conclusions

Hydrous ferric oxide was prepared and used to remove PFOS from aqueous solution. The results of ionic strength adsorption tests demonstrated that site competition and bridge enhancement were the predominant adsorption mechanism. FTIR and XPS analyses indicated the presence of a wide variety of functional groups for the HFO bonding. Electronic attraction was formed between the –COOH groups of PFOS and groups of Fe–OH and halogenated hydrocarbons on the HFO surface, which favored the sorption of PFOS. Fluorinion, chloridion, nitrate, and sulfate show strong interfering effect on PFOS adsorbed in HFO. Therefore, PFOS can be effective adsorbed onto HFO in water, then the transfer behavior of PFOS would be affected by HFO transfer in water with solution condition variation.

Funding

The research was supported by National Natural Science Foundation of China (51609001, 51809001 and 51709002), National Students' Innovation and Entrepreneurship Training Program (201810364206 and 2020ysj-70).

References

[1] J.P. Giesy, K. Kannan, Peer reviewed: perfluorochemical surfactants in the environment, Environ. Sci. Technol., 36 (2002) 146A–152A.
[2] T. Wang, Y. Wang, C. Liao, Y. Cai, G. Jiang, Perspectives on the inclusion of perfluorooctane sulfonate into the Stockholm Convention on persistent organic pollutants, Environ. Sci. Technol., 43 (2009) 5171–5175.
[3] J.B.N. Mudumbi, S.K.O. Ntwampe, F.M. Muganza, J.O. Okonkwo, Perfluorooctanoate and perfluorooctane sulfonate in South African river water, Water Sci. Technol., 69 (2014) 185–194.
[4] X. Liu, H. Pang, X. Liu, Q. Li, N. Zhang, L. Mao, M. Qiu, B. Hu, H. Yang, X. Wang, Orderly porous covalent organic frameworks-based materials: superior adsorbents for pollutants removal from aqueous solutions, Innovation, 2 (2021) 100076, doi: 10.1016/j.xinn.2021.100076.
[5] Q. Yu, R. Zhang, S. Deng, J. Huang, G. Yu, Sorption of perfluorooctane sulfonate and perfluorooctanoate on activated carbons and resin: kinetic and isotherm study, Water Res., 43 (2009) 1150–1158.
[6] M. Sundstrom, J. Bogdanska, H.V. Pham, V. Athanasios, S. Nobel, A. McAlees, J. Eriksson, J.W. DePierre, A. Bergman, Radiosynthesis of perfluorooctanesulfonate (PFOS) and perfluorobutanesulfonate (PFBS), including solubility, partition and adhesion studies, Chemosphere, 87 (2012) 865–871.
[7] L. Zhang, J. Liu, J. Hu, C. Liu, W. Guo, Q. Wang, H. Wang, The inventory of sources, environmental releases and risk assessment for perfluorooctane sulfonate in China, Environ. Pollut., 165 (2012) 193–198.
[8] A.G. Paul, K.C. Jones, A.J. Sweetman, A first global production, emission, and environmental inventory for perfluorooctane sulfonate, Environ. Sci. Technol., 43 (2009) 386–392.
[9] V.T. Nguyen, K.Y.-H. Gin, R. Martin, L. Changhui, Occurrence, fate, and fluxes of perfluorochemicals (PFCs) in an urban catchment: Marina Reservoir, Singapore, Water Sci. Technol., 66 (2012) 2439–2446.
[10] J.N. Uwayezu, L.W.Y. Yeung, M. Bäckström, Sorption of PFOS isomers on goethite as a function of pH, dissolved organic matter (humic and fulvic acid) and sulfate, Chemosphere, 233 (2019) 896–904.
[11] V.P. Beskoski, S. Takemine, T. Nakano, L.S. Beskoski, G. Gojgic-Cvijovic, M. Ilic, S. Miletic, M.M. Vrvic, Perfluorinated compounds in sediment samples from the wastewater canal of Pancevo (Serbia) industrial area, Chemosphere, 91 (2013) 1408–1415.
[12] H.B. Jin, Y.F. Zhang, L.Y. Zhu, J.W. Martin, Isomer profiles of perfluoroalkyl substances in water and soil surrounding a Chinese Fluorochemical Manufacturing Park, Environ. Sci. Technol., 49 (2015) 4946–4954.
[13] J. Milinovic, S. Lacorte, M. Vidal, A. Rigol, Sorption behaviour of perfluoroalkyl substances in soils, Sci. Total Environ., 511 (2015) 63–71.
[14] C.P. Higgins, R.G. Luthy, Sorption of perfluorinated surfactants on sediments, Environ. Sci. Technol., 40 (2006) 7251–7256.
[15] A.M. Becker, S. Gerstmann, H. Frank, Perfluorooctanoic acid and perfluorooctane sulfonate in the sediment of the Roter Main River, Bayreuth, Germany, Environ. Pollut., 156 (2008) 818–820.
[16] D. Peak, G.W. Luthe, D.L. Sparks, ATR-FTIR spectroscopic studies of boric acid adsorption on hydrous ferric oxide, Geochem. Cosmochim. Acta, 67 (2003) 2551–2560.
[17] C. Hyacinthe, P.V. Cappellen, An authigenic iron phosphate phase in estuarine sediments: composition, formation and chemical reactivity, Mar. Chem., 91 (2004) 227–251.
[18] B.M. Jovanovic, V.L. Vukasinovic-Pesic, L.V. Rajakovic, Enhanced arsenic sorption by hydrated iron(III) oxide-coated materials-mechanism and performances, Water Environ. Res., 83 (2011) 498–506.
[19] L. Huo, D. Huang, X. Zeng, S. Su, Y. Wang, L. Bai, C. Wu, Arsenic availability and uptake by edible rape (*Brassica campestris* L.) grown in contaminated soils spiked with carboxymethyl cellulose-stabilized ferrihydrite nanoparticles, Environ. Sci. Pollut. Res., 25 (2018) 15080–15088.
[20] Y. Xu, X. Sun, Q. Zhang, X. Li, Z. Yan, Iron plaque formation and heavy metal uptake in *Spartina alterniflora* at different tidal levels and waterlogging conditions, Ecotoxicol. Environ. Saf., 153 (2018) 91–100.

[21] J. Zang, T. Wu, H. Song, N. Zhou, S. Fan, Z. Xie, J. Tang, Removal of tetracycline by hydrous ferric oxide: adsorption kinetics, isotherms, and mechanism, Int. J. Environ. Res. Public Health., 16 (2019b) 4580–4592.
[22] N. Khan, B. Seshadri, N. Bolan, C.P. Saint, M.B. Kirkham, S. Chowdhury, N. Yamaguchi, D.Y. Lee, G. Li, A. Kunhikrishnan, F. Qi, R. Karunanithi, R. Qiu, Y.G. Zhu, C.H. Syu, Root iron plaque on wetland plants as a dynamic pool of nutrients and contaminants, Adv. Agron., 138 (2016) 1–96.
[23] Y. Tai, N.F.Y. Tam, R. Wang, Y. Yang, J. Lin, J. Wang, Y. Yang, L. Li, Y. Sun, Iron plaque formation on wetland-plant roots accelerates removal of water-borne antibiotics, Plant Soil, 433 (2018) 323–338.
[24] C.Y. Tang, F.Q. Shiang, D. Gao, C.S. Criddle, J.O. Leckie, Effect of solution chemistry on the adsorption of perfluorooctane sulfonate onto mineral surfaces, Water Res., 44 (2010b) 2654–2662.
[25] H. Zhang, M. Elskens, G. Chen, L. Chou, Phosphate adsorption on hydrous ferric oxide (HFO) at different salinities and pHs, Chemosphere, 225 (2019) 352–359.
[26] H.M. Jang, S. Yoo, Y.K. Choi, S. Park, E. Kan, Adsorption isotherm, kinetic modeling and mechanism of tetracycline on *Pinus taeda*-derived activated biochar, Bioresour. Technol., 259 (2018) 24–31.
[27] W. Wang, Z. Du, S. Deng, M. Vakili, L. Ren, P. Meng, G. Yu, Regeneration of PFOS loaded activated carbon by hot water and subsequent aeration enrichment of PFOS from eluent, Carbon, 134 (2018) 199–206.
[28] C. Wang, H. Wang, Y. Cao, Pb(II) sorption by biochar derived from *Cinnamomum camphora* and its improvement with ultrasound-assisted alkali activation, Colloids Surf., A, 556 (2018) 177–184.
[29] C. Wang, R. Huang, R. Sun, Green one-spot synthesis of hydrochar supported zero-valent iron for heterogeneous Fenton-like discoloration of dyes at neutral pH, J. Mol. Liq., 320 (2020) 114421, doi: 10.1016/j.molliq.2020.114421.
[30] S. Fan, Y. Wang, Z. Wang, J. Tang, J. Tang, X. Li, Removal of methylene blue from aqueous solution by sewage sludge-derived biochar: adsorption kinetics, equilibrium, thermodynamics and mechanism, J. Environ. Chem. Eng., 5 (2017) 601–611.
[31] H. Qiu, W. Ni, H. Zhang, K. Chen, J. Yu, Fabrication and evaluation of a regenerable HFO-doped agricultural waste for enhanced adsorption affinity towards phosphate, Sci. Total Environ., 703 (2020) 135493.1–135493.11, doi: 10.1016/j.scitotenv.2019.135493.
[32] X. Chen, G. Chen, L. Chen, Y. Chen, J. Lehmann, M.B. McBride, A.G. Hay, Adsorption of copper and zinc by biochars produced from pyrolysis of hardwood and corn straw in aqueous solution, Bioresour. Technol., 102 (2011) 8877–8884.
[33] M.G. Sujana, A. Mishra, B.C. Acharya, Hydrous ferric oxide doped alginate beads for fluoride removal: adsorption kinetics and equilibrium studies, Appl. Surf. Sci., 270 (2013) 767–776.
[34] Y. Xing, Q. Li, X. Chen, X. Fu, L. Ji, J. Wang, Q. Zhang, Different transport behaviors and mechanisms of perfluorooctanoate (PFOA) and perfluorooctane sulfonate (PFOS) in saturated porous media, J. Hazard. Mater., 402 (2021) 123435, doi: 10.1016/j.jhazmat.2020.123435.
[35] L. Hu, G. Zhang, M. Liu, Q. Wang, P. Wang, Enhanced degradation of Bisphenol A (BPA) by peroxymonosulfate with Co_3O_4-Bi_2O_3 catalyst activation: Effects of pH, inorganic anions, and water matrix, Chem. Eng. J., 338 (2018) 300–310.
[36] J.M. Jian, C. Zhang, F. Wang, X. Lu, F. Wang, E.Y. Zeng, Effect of solution chemistry and aggregation on adsorption of perfluorooctanesulphonate (PFOS) to nano-sized alumina, Environ. Pollut., 251 (2019) 425–433.
[37] X. Hao, W.A. Spieker, J.R. Regalbuto, A further simplification of the revised physical adsorption (RPA) model, J. Colloid Interface Sci., 267 (2003) 259–264.
[38] F. Wang, C. Liu, K. Shih, Adsorption behavior of perfluorooctanesulfonate (PFOS) and perfluorooctanoate (PFOA) on boehmite, Chemosphere, 89 (2012) 1009–1014.
[39] Q. Zhang, S. Deng, G. Yu, J. Huang, Removal of perfluorooctane sulfonate from aqueous solution by cross-linked chitosan beads: sorption kinetics and uptake mechanism, Bioresour. Technol., 102 (2011) 2265–2271.
[40] S. Deng, Q. Yu, J. Huang, G. Yu, Removal of perfluorooctane sulfonate from wastewater by anion exchange resins: effects of resin properties and solution chemistry, Water Res., 44 (2010) 5188–5195.
[41] Z. Du, S. Deng, Y. Bei, Q. Huang, B. Wang, J. Huang, G. Yu, Adsorption behavior and mechanism of perfluorinated compounds on various adsorbents—a review, J. Hazard. Mater., 274 (2014) 443–454.
[42] F. Xiao, X. Zhang, L. Penn, J.S. Gulliver, M.F. Simcik, Effects of monovalent cations on the competitive adsorption of perfluoroalkyl acids by kaolinite: experimental studies and modeling, Environ. Sci. Technol., 45 (2011) 10028–10035.
[43] C. You, C. Jia, G. Pan, Effect of salinity and sediment characteristics on the sorption and desorption of perfluorooctane sulfonate at sediment-water interface, Environ. Pollut., 158 (2010) 1343–1347.
[44] F. Wang, K. Shih, Adsorptionof perfluorooctanesulfonate (PFOS) and perfluorooctanoate (PFOA) on alumina: influence of solution pH and cations, Water Res., 45 (2011) 2925–2930.
[45] H. Wijnja, C.P. Schulthess, Vibrational spectroscopy study of selenate and sulfate adsorption mechanisms on Fe and Al (hydr) oxide surfaces, J. Colloid Interface Sci., 229 (2000) 286–297.
[46] Y. Tang, X. Guan, J. Wang, N. Gao, M.R. McPhail, C.C. Chusuei, Fluoride adsorption onto granular ferric hydroxide: effects of ionic strength, pH, surface loading, and major co-existing anions, J. Hazard. Mater., 171 (2009) 774–779.
[47] X. Gao, J. Chorover, Adsorption of perfluorooctanoic acid and perfluorooctanesulfonic acid to iron oxide surfaces as studied by flow-through ATR-FTIR spectroscopy, Environ. Chem., 9 (2012) 148–157.
[48] X. Zhao, J. Wang, F. Wu, T. Wang, Y. Cai, Y. Shi, G. Jiang, Removal of fluoride from aqueous media by Fe_3O_4@$Al(OH)_3$ magnetic nanoparticles, J. Hazard. Mater., 173 (2010) 102–109.
[49] C. Xu, H. Chen, F. Jiang, Adsorption of perflourooctane sulfonate (PFOS) and perfluorooctanoate (PFOA) on polyaniline nanotubes, Colloids Surf., A, 479 (2015) 60–67.
[50] Q. Yu, S. Deng, G. Yu, Selective removal of perfluorooctane sulfonate from aqueous solution using chitosan-based molecularly imprinted polymer adsorbents, Water Res., 42 (2008) 3089–3097.
[51] Y. Liu, D.W. Blowes, C.J. Ptacek, L.G. Groza, Removal of pharmaceutical compounds, artificial sweeteners, and perfluoroalkyl substances from water using a passive treatment system containing zero-valent iron and biochar, Sci. Total Environ., 691 (2019) 165–177.
[52] K.M. Doke, E.M. Khan, Equilibrium, kinetic and diffusion mechanism of Cr(VI) adsorption onto activated carbon derived from wood apple shell, Arabian J. Chem., 10 (2017) S252–S260.
[53] H. Anjum, K. Johari, N. Gnanasundaram, A. Appusamy, M. Thanabalan, Impact of surface modification on adsorptive removal of BTX onto activated carbon, J. Mol. Liq., 280 (2019) 238–251.
[54] L. Leng, X. Yuan, H. Huang, J. Shao, H. Wang, X. Chen, G. Zeng, Bio-char derived from sewage sludge by liquefaction: characterization and application for dye adsorption, Appl. Surf. Sci., 15 (2015) 223–231.
[55] S. Fan, J. Tang, Y. Wang, H. Li, H. Zhang, J. Tang, Z. Wang, X. Li, Biochar prepared from co-pyrolysis of municipal sewage sludge and tea waste for the adsorption of methylene blue from aqueous solutions: kinetics, isotherm, thermodynamic and mechanism, J. Mol. Liq., 220 (2016) 432–441.
[56] M.S. Onyango, Y. Kojima, O. Aoyi, E.C. Bernardo, H. Matsuda, Adsorption equilibrium modeling and solution chemistry dependence of fluoride removal from water by trivalent-cation-exchanged zeolite F-9, J. Colloid Interface Sci., 279 (2004) 341–350.
[57] L. Liu, Y. Lin, Y. Liu, H. Zhu, Q. He, Removal of methylene blue from aqueous solutions by sewage sludge based granular

activated carbon: adsorption equilibrium, kinetics, and thermodynamics, J. Chem. Eng. Data, 58 (2013) 2248–2253.
[58] F. Wang, K. Shih, J.O. Leckie, Effect of humic acid on the sorption of perfluorooctane sulfonate (PFOS) and perfluorobutane sulfonate (PFBS) on boehmite, Chemosphere, 118 (2015) 213–218.
[59] E. Wibowo, M. Rokhmat, Sutisna, Khairurrijal, M. Abdullah, Reduction of seawater salinity by natural zeolite (Clinoptilolite): adsorption isotherms, thermodynamics and kinetics, Desalination, 409 (2017) 146–156.
[60] B.O. Fagbayigbo, B.O. Opeolu, O.S. Fatoki, T.A. Akenga, O.S. Olatunji, Removal of PFOA and PFOS from aqueous solutions using activated carbon produced from *Vitis vinifera* leaf litter, Environ. Sci. Pollut. Res., 24 (2017) 13107–13120.
[61] W. Guo, S. Huo, J. Feng, X. Lu, Adsorption of perfluorooctane sulfonate (PFOS) on corn straw-derived biochar prepared at different pyrolytic temperatures, J. Taiwan Inst. Chem. Eng., 78 (2017) 265–271.

Supporting information

S1. Adsorption kinetics equations

The pseudo-first-order equation is described as Eq. (2) [S1]:

$$q_t = q_e\left(1-\exp\left(-k_1 t\right)\right) \tag{2}$$

The pseudo-second-order equation is described as Eq. (3) [S2]:

$$q_t = \frac{k_2 q_e^2 t}{\left(1+k_2 q_e t\right)} \tag{3}$$

where q_t (mg g^{-1}) and q_e (mg g^{-1}) are the adsorption amounts at time t (min) and at equilibrium, respectively. k_1 (min^{-1}) and k_2 (g (mg min)$^{-1}$) represent reaction rate constants of the pseudo-first-order and pseudo-second-order models, respectively.

The two-compartment first-order model is expressed as Eq. (4) [S3]:

$$q_t = q_e\left[1-\left(F_{\text{fast}}\exp\left(-t\times k_{\text{fast}}\right)+ F_{\text{slow}}\exp\left(-t\times k_{\text{slow}}\right)\right)\right] \tag{4}$$

where parameters of F_{fast} and F_{slow} are the mass fractions of "fast" and "slow" compartments, respectively, and F_{fast} + F_{slow} = 1. Parameters of F_{fast} (min^{-1}) and F_{slow} (min^{-1}) are the first-order rate constants for transfer into "fast" and "slow" compartments, respectively, of hydrous ferric oxide by the perfluorooctane sulfonate model.

The intraparticle diffusion model is expressed as Eq. (5) [S4]:

$$q_t = K_i \times t^{0.5} + C \tag{5}$$

where K_i (mg g^{-1} min$^{0.5}$) is the intraparticle diffusion rate constant, and C (mg g^{-1}), a constant, is related to the boundary layer thickness.

S2. Adsorption isotherm equations

The Langmuir adsorption isotherm is described as Eq. (6) [S5]:

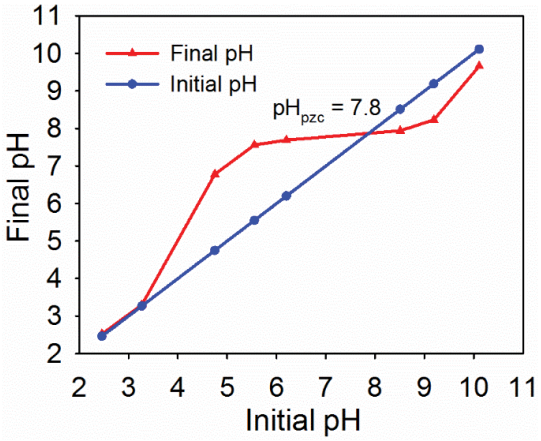

Fig. S1. pH$_{PZC}$ of hydrous ferric oxide.

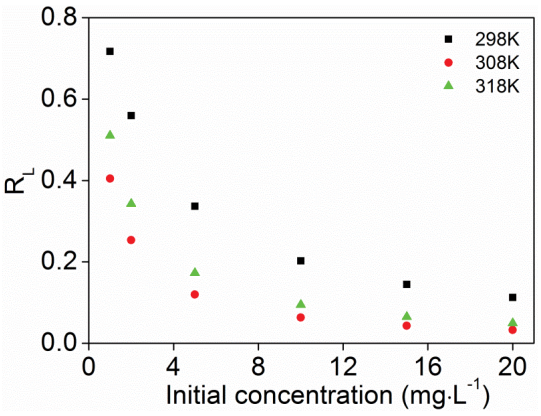

Fig. S2. Effect of initial perfluorooctane sulfonate concentration and temperature on the Langmuir equilibrium factor (R_L) for adsorption onto hydrous ferric oxide.

$$q_e = \frac{q_m K_L C_e}{\left(1+K_L C_e\right)} \tag{6}$$

The Freundlich adsorption isotherm is described as Eq. (7) [S6]:

$$q_e = K_F C_e^{1/n} \tag{7}$$

where q_e (mg g^{-1}) is the equilibrium adsorption capacity, and q_m (mg) is the maximum adsorption capacity. K_F ((L g^{-1})$^{1/n}$) and K_L (L g^{-1}) are the Freundlich and Langmuir adsorption isotherm constants, respectively; 1/n is the adsorption affinity constant.

The Temkin isotherm model is described as Eq. (8) [S7]:

$$q_e = \frac{RT}{B_T \ln\left(A_T\right)} + \frac{RT}{B_T \ln\left(C_e\right)} \tag{8}$$

where A_T is the equilibrium bond constant related to the maximum energy of the bond. B_T is the Temkin constant concerned with the sorption heat. R is the universal gas constant, and T is the temperature in terms of Kelvin.

The Dubinin–Radushkevitch isotherm equation is described as Eqs. (9)–(11) [S8]:

$$\ln q_e = \ln q_m - \beta_D \varepsilon^2 \tag{9}$$

$$\varepsilon = RT \ln\left(1 + \frac{1}{C_e}\right) \tag{10}$$

$$E_a = \frac{1}{\sqrt{2\beta}} \tag{11}$$

where β is the activity coefficient related to the mean free energy of sorption (mol^2 J^{-2}), and ε is the Polanyi potential. E_a is the free energy of the transfer of adsorbate from solution to the sorbent surface.

References

[S1] S.K. Lagergren, About the theory of so-called adsorption of soluble substances, Kungliga Svenska Vetenskapsakademiens Handlingar, 24 (1898) 1–39.

[S2] G. Blanchard, M. Maunaye, G. Martin, Removal of heavy metals from waters by means of natural zeolites, Water Res., 18 (1984) 1501–1507.

[S3] Y. Cherruault, V.B. Sarin, Identification of pharmacokinetic parameters of two compartment open model with first order absorption, Int. J. Bio-Med. Comput., 16 (1985) 127–133.

[S4] S. Fan, Y. Wang, Z. Wang, J. Tang, X. Li, Removal of methylene blue from aqueous solution by sewage sludge-derived biochar: adsorption kinetics, equilibrium, thermodynamics and mechanism, J. Environ. Chem. Eng., 5 (2017) 601–611.

[S5] I. Langmuir, The adsorption of gases on plane surfaces of glass, mica and platinum, J. Am. Chem. Soc., 40 (1918) 1361–1403.

[S6] H. Freundlich, Über die Adsorption in Lösungen, Zeitschrift For Physikalische Chemie, 57U (1907) 385–470.

[S7] L. Leng, X. Yuan, H. Huang, J. Shao, H. Wang, X. Chen, G. Zeng, Bio-char derived from sewage sludge by liquefaction: characterization and application for dye adsorption, Appl. Surf. Sci., 346 (2015) 223–231.

[S8] M.S. Onyango, Y. Kojima, O. Aoyi, E.C. Bernardo, H. Matsuda, Adsorption equilibrium modeling and solution chemistry dependence of fluoride removal from water by trivalent-cation-exchanged zeolite F-9, J. Colloid Interface Sci., 79 (2004) 341–350.